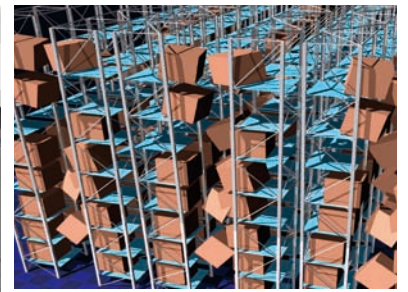# TSUBAME
ESJ.

Numerical simulation of air/water multiphase flows
for ceramic sanitary ware design by multiple GPUs

A Hybrid Quantum-Classical Simulation
study on the Li Diffusion
in Li-Graphite Intercalation Compounds

A Large-scale Simulation on CFD
in Construction Industry

Estimation of strong ground motion and
damage of indoor objects during giant earthquake

Numerical simulation of air/water multiphase flows for ceramic sanitary ware design by multiple GPUs

Akio Ikebata* Shinya Yoshida* Feng Xiao**
*TOTO LTD., Production technology center   ** Tokyo Institute of Technology, Department of energy sciences

We have been developing an in-house CAE air/water two-phase numerical code for various purposes in design and manufacturing of plumbing products such as ceramic sanitary wares. In order to re-produce the complex interfacial flows of air and water with adequate accuracy, large scale computations are required with reliable numerical model, which is of great challenge. To this end, we have made efforts to improve the numerical schemes and port the code to the GPU platforms to accelerate the large scale computations for real-case applications. We have implemented large-scale simulation on the TSUBAME2.0 supercomputer by making effective use of the GPGPU architecture, and achieved significant improvement in both computational performance and simulation results.

Introduction 1

Being a world-wide leading company, TOTO manufactures and provides a wide spectrum of household products, such as ceramic sanitary wares, bathroom and kitchen fittings. Facing the increasing demands for saving energy and water, TOTO has always targeted the high standard in this respect for the design and manufacture processes. For this purpose, development and effective use of accurate and reliable CFD (computational fluid dynamics) technology as a CAE design tool become extremely necessary.

In the numerical models which are based on Navier-Stokes equations and explicitly resolve the moving interfaces of gas/liquid multiphase flows, like those involving gas bubbles and liquid films, the advection scheme plays a crucial role for getting stable and accurate numerical solutions.

MUSCL scheme [10] is perhaps the most representative advection scheme, and has been widely adopted in the commercial CFD codes. MUSCL scheme is essentially based on the linear reconstruction and makes use of upwinding and limiters to get stable and monotonic numerical solutions. As we will show later, MUSCL scheme appears to be too diffusive to resolve the fine structures which always associate large jumps and discontinuities in flow fields. Moreover, our experiences show that MUSCL scheme usually failed in reproducing reasonable results in violent liquid splashing problems where the MUSCL scheme seems to be more grid dependent even the physical problem is geometrically isotropic.

As a completely different alternative, the CIP [1-3] scheme is a highly accurate advection scheme which is particularly more robust and less grid-dependent. CIP scheme uses multi-moment concept and updates not only the point value but also the gradients of the physical fields. CIP scheme has third-order accuracy and can be combined with the semi-Lagrangian scheme to get computational efficiency. However the original CIP scheme doesn't ensure numerical conservation, which may turn out to be a serious problem in many applications, such as interfacial multi-phase flows where mass (or volume) conservation is a basic requirement to resolve small droplets, bubbles and water films.

For the purpose of numerical simulations for real-case product design, we have devised a conservative variant of the CIP method, so-called UTI-VSIAM3 scheme [4], and developed an accurate and efficient numerical code for two-phase interfacial multiphase flows. The code has been ported to GPGPU hardware, and tuned on the TSUBAME 2.0 supercomputer for large scale high-resolution simulations.

This paper presents our recent efforts to improve the numerical schemes for multi-phase interfacial flows and to implement the code on GPGPU architecture.

The numerical scheme for advection 2

We consider the advection equation

$$\frac{\partial \phi}{\partial t} + u\frac{\partial \phi}{\partial x} + v\frac{\partial \phi}{\partial y} + w\frac{\partial \phi}{\partial z} = 0 \qquad (1)$$

where φ denotes the advected quantity, and u,v,w, the components of the velocity field.

As presented in [5], a one dimensional conservative CIP scheme, CIP-CSL (conservative semi-Lagrangian) scheme, uses at least more than two kinds of moments as the computational variables. In order to make the numerical model computationally efficient, we construct the multidimensional formulation based on two kinds of moments [6], i.e. VIA (Volume Integrated Average) and

SIA (Surface Integrated Average) as shown in Fig.1 for 3-dimensional model. The one dimensional conservative CIP schemes can be used as the building block through a splitting procedure. So, a reconstruction of either quadratic polynomial or rational function can be build over a single cell. This local reconstruction with adequate accuracy is very important to resolve complex flow structures in presence of discontinuities, such as multi-phase flows. In practice, the one-dimensional scheme is consistently applied to SIA and VIA moments in each direction respectively. The SIA is updated by a semi-Lagrangian solution, while the VIA is computed from a finite volume formulation of flux form that guarantees rigorously numerical conservation. This formulation, so-called VSIAM3 (Volume/Surface Integrated Average based Multi-Moment Method), has been further extended to be a general solver for fluid dynamics [6].
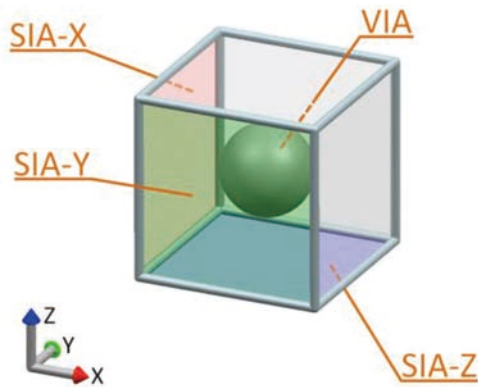
Figure 1 The definition of VIA and SIA moments

In the original VSIAM3 formulation, the one-dimensional building block is used in a straightforward way for multi-dimensional calculation. Alternatively, a multi-dimensional updating can constructed as follows.

Shown in Fig.2, we consider the advection computation of SIA-X. The advection equation is divided equivalently into next two-step form.

Step 1：

$$\frac{\partial \phi}{\partial t} + u \frac{\partial \phi}{\partial x} = 0 \qquad (2)$$

Step 2：

$$\frac{\partial \phi}{\partial t} = -\frac{\partial v\phi}{\partial y} - \frac{\partial w\phi}{\partial z} + \phi\left(\frac{\partial v}{\partial y} + \frac{\partial w}{\partial z}\right) \quad (3)$$

The one-dimensional scheme is firstly used to solve equation (2) in x direction to get the intermediate value for SIA-X, the SIA for the surface element normal to x direction. The intermediate value of SIA-X is then used to compute the spatial discretizations for equation (3) where a simple central difference is applied. The SIA-X is then updated to the new time step. This procedure applies to SIA-Y and SIA-Z. Given the SIA values on all surface elements, the VIA can be updated by a finite volume formulation. The scheme is called UTI-VSIAM3 (Unsplit Time Integration VSIAM3), which essentially ensures that the updating of the SIAs in different directions are conducted in a symmetrical manner [4].
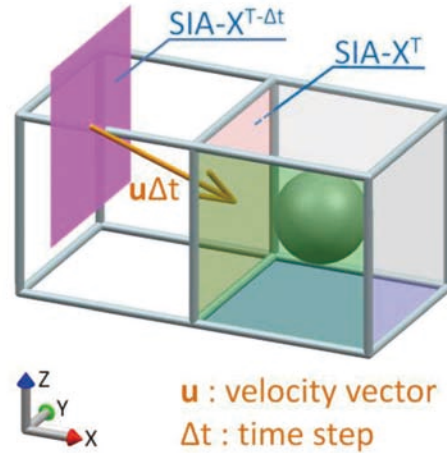
Figure 2 Multi-dimensional updating of the SIA moment.

We evaluated the advection schemes by transporting a "T" shape initial distribution via a pure anti-clock rotational velocity field. The numerical results after one revolution are displayed in Fig.3. The results from both original VSIAM3 and UTI-VSIAM3 are much superior to the MUSCL scheme. For this pure advection test, there is not visible difference in the numerical solutions between the original VSIAM3 and UTI-VSIAM3 though, the multi-dimensional updating in UTI-VSIAM3 can be expected beneficial in real-case applications.
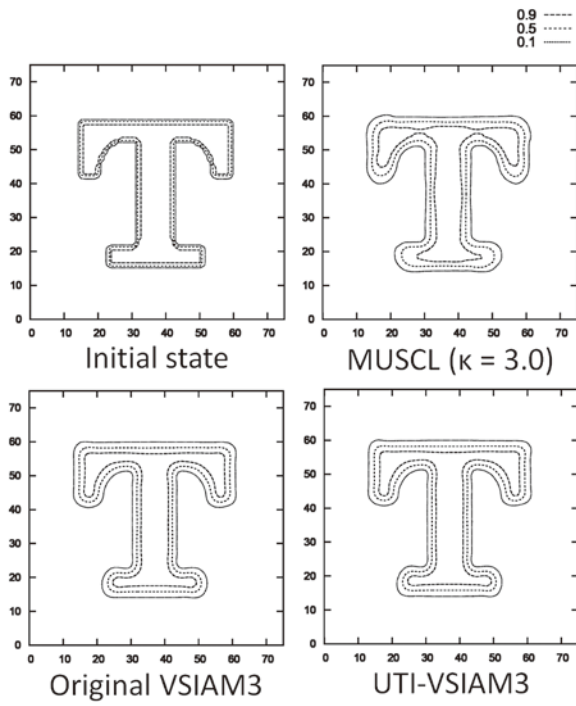
Figure 3 Advection benchmark tests.

STAA (Surface Tracking by Artificial Anti-diffusion)[7] scheme. STAA scheme combines the conservative CIP (CIP-CSL) scheme with an anti-diffusion post-processing step to the VOF function. The CIP-CSL scheme is able to compute the advection transport with adequate fidelity. However, same as other high order schemes based on finite grid resolutions, the advected field is usually smeared out due to numerical diffusion. To maintain the steepness of the VOF function through the whole computation procedure, correction is added to the VOF field after the advection step. To this end, a level set function is generated from the VOF field, which then gives the normal direction of the interface. The numerical diffusion from the advection calculation is corrected through an artificial compression in the normal direction of the interface, which improves the geometrical faithfulness of the moving interface. The STAA scheme is efficient and very easy to use. Fig.4 shows the numerical results for the aforementioned advection test. The STAA scheme gives much superior result than the PLIC VOF scheme, especially in the geometrical shape of the transported field. The thickness of transitional layer in the STAA calculation is adjustable for practical use. Our experience in real-case applications shows that the STAA scheme is very stable, robust and reliable.
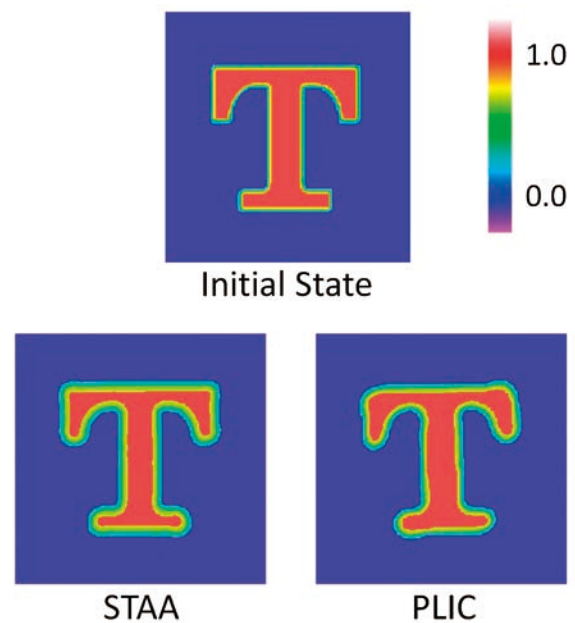
Interface tracing method

3

Volume fraction is a well suited variable to identify the interface in multiphase flow simulation. The VOF (Volume of Fluid) method uses the volume fraction (VOF function) for capturing moving interfaces. Different from other particle-based front tracking methods, VOF method is able to directly compute complex interfaces of arbitrary topological changes, such as breaking and merging of the interfaces. Moreover, VOF schemes automatically guarantees the conservation of the VOF function, which is of great importance for real-case applications and makes the VOF among the most popular methods for interface capturing/tracking. The conventional VOF schemes adopt geometrical reconstructions which are required then in estimating the numerical fluxes to update the VOF function. Usually a PLIC type reconstruction[9] is needed to give adequate numerical accuracy. However, the PLIC algorithm is complicated and not easy to implement.

In order to calculate moving interfaces more accurately and efficiently, we have devised an interface capturing scheme,


Figure 4 Interface transport tests.

Porting to GPGPU architecture 4

Our numerical code is based on a fractional step solution procedure. Following the numerical steps for advection, diffusion, gravity, surface tension and other physical processes, a pressure projection step is used to update the velocity field to the new time level. All computations can be carried out in an explicit manner except the Poisson equation for pressure projection. The whole code is organized so as to be suitable for vector processing. Thus, there is not substantial barrier to run the code on a parallel environment. In order to implement the code on parallel machines with distributed memories and GPGPU accelerators, we have re-written the code thoroughly with MPI and OpenCL libraries. Although our current target GPU is nVIDIA CUDA architecture, we make use of OpenCL to allow the code flexibility to be portable across a variety of GPUs and CPUs, like AMD and Intel's or other new devices in near future. It is known that OpenCL usually results in lower performance about 10% compared to CUDA. Improvement has been achieved by compiling the code with CUDA Driver API conversion to utilize the native CUDA functions. Furthermore, we have defined some wrapper functions to simplify the OpenCL instructions in the fluid code.

Fig.5 plots the comparison of the elapse time between CPU and GPU. Double precision is used to guarantee the iteration converging with an adequate accuracy. 8 times speed-up is achieved on single core and nearly 10 times speed-up on 4 cores.

Fig.6 shows an example of simulating fluid flow in a ceramic sanitary ware. The water flowing on the solid surface of complex geometry, as well as the interaction with floating bodies, was reasonably reproduced. The floating bodies are represented by the volume fraction of solid, similar to that used for distinguishing air/water surface[8]. Again, the level set function is used to compute the distances among the solid bodies, which is then used in the calculations of contact and rebounce model. All of these are coded in a completely portable way to any parallel GPGPU architectures. So, we can carry out directly fluid-solid interaction simulations (including gas, liquid and solid) of a relatively large grid size even on a personal computer with low-cost GPU cards, which was thought impossible unless a supercomputer would be available before. Establishing such a system is particularly important for the practical use in product-design process, where numbers of case studies can be conducted simultaneously on several PCs within acceptable computational time.
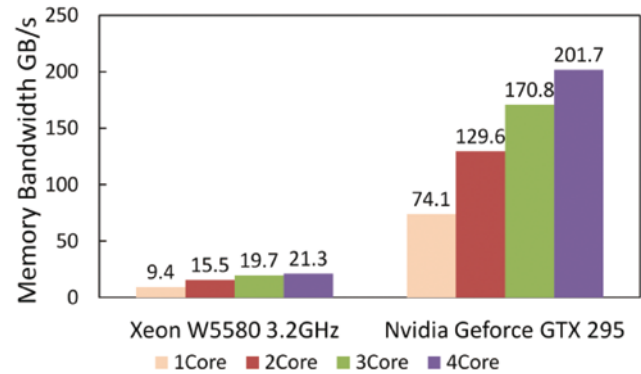
Figure 5 Comparison of the execution time of PCG Poisson solver on CPU and GPU.

Figure 6 The simulation results of the multiphase flows containing gas, liquid and solid.

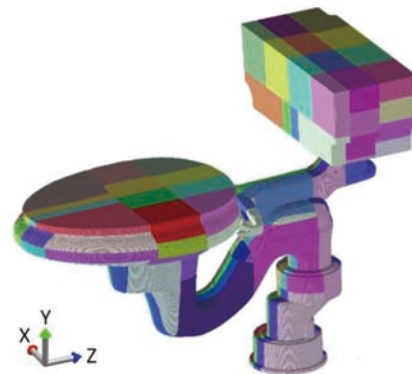## Implementation on TSUBAME2.0 5

Since water-saving increasingly becomes a key requirement for all plumbing fixtures, how to design products that use less water and have high washing efficiency is the central task we are facing currently. From the CAE point, we need to resolve the thin water film and small bubbles in numerical simulations, which can be only realized with finer grid resolution. For example, a mesh-spacing less than 1mm is required to resolve a film with 2mm thickness. Thus, over ten million mesh elements are usually needed for the whole system, which is quite challenging for a PC-based hardware. So, we have implemented our code on TSBAME2.0 supercomputer in Tokyo Institute of Technology for large scale simulations of multiphase interface flows.
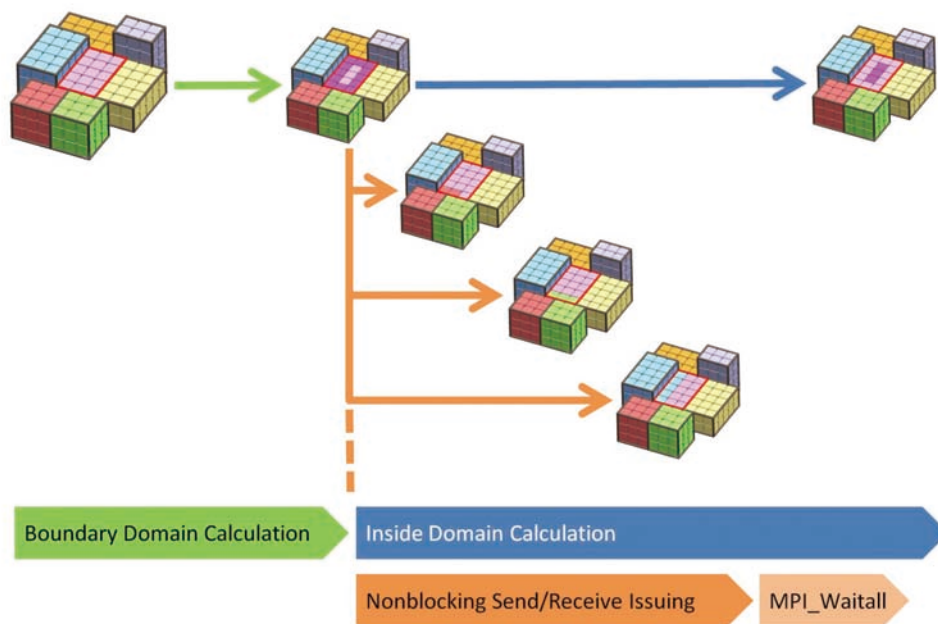
As the computation performance of a single GPU is significantly superior to a single CPU, the data communication overhead in parallel processing becomes the major barrier to get high parallel efficiency. Because the flow path structure of the ceramic ware is very complex, it is not easy to get a satisfactory parallel scalability if the parallel partition is decomposed along the flow path. On the other hand, a regular 3D Cartesian decomposition will include a large number of elements that are not actually used in the flow computation. We have finally adopted a flexible 3D partition as shown in Fig.7. All flow path elements are decomposed along z, y and x directions automatically, which allows the computational load to be evenly assigned to each process. Consequently, the halo regions might be not exactly matched among the neighboring domains, which complicates the data transfer for parallel processing. We use asynchronous communication for data transfer based on a pre-determined send/receive route. To save the wall-clock time, we overlap data communication with computation as shown in Fig.8. All data transfers are finally synchronized by MPI_Waitall function.

Fig.9 shows the parallel speedup of the Poisson solver for real-case application where 150 million mesh elements were used. 80 times speedup is obtained on 100 GPUs and 100 times on 150 GPUs, which shows a reasonable parallel efficiency of the present code. Since the Poisson solver is the most computationally expensive part in the numerical model for fluid dynamics, the parallel performance shown above reveals that the parallelization of the code for GPU architectures are quite promising for large scale simulations.


Figure 7 Three dimensional parallel partition. (conceptual rendering)

Boundary Domain Calculation

Inside Domain Calculation

Nonblocking Send/Receive Issuing

MPI_Waitall

Figure 8 Overlapping data communication.

Fig.10 displays a real-case simulation of water flows in a sanitary ware. All results were also visualized on TSUBAME2.0 with POV-Ray. Being in agreement with the real design conditions, the water initially stored in the tank was released with the amount controlled by the drain valve. The water flushing through the whole flow path was simulated. The fine liquid structures and the entrainment of massive bubbles were adequately captured. The large scale simulation on TSUBAME2.0 allows us to explicitly resolve the bubble, thin film and spray of millimeter size, which drastically improves the accuracy and reliability of the numerical simulations for the flushing process of sanitary set.
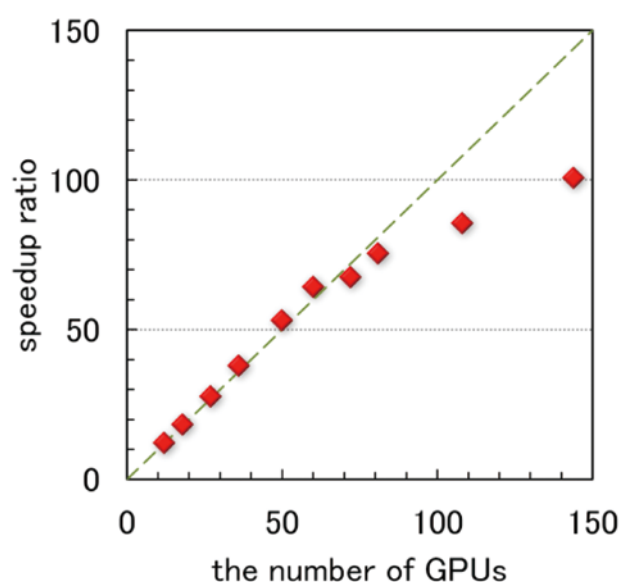
Figure 9 Speedup of PCG solver by multi-GPUs.
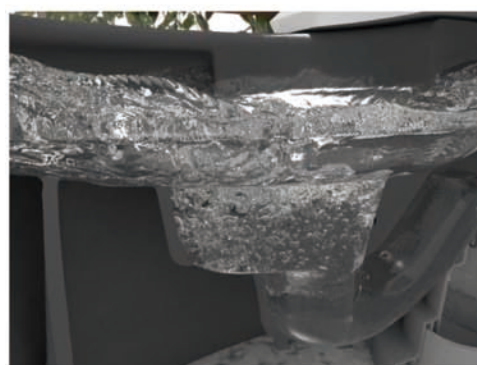
Figure 10 Real case simulation of sanitary set by TSUBAME 2.0 supercomputer.

Summary 6

For accurate and efficient numerical simulations of air/water multiphase flows for sanitary ware design, we have developed a reliable numerical model based on the UTI-VSIAM3 and STAA schemes. The code has been parallelized by optimizing the load balance for the effective flow path region via a flexible three-dimensional domain decomposition, and ported to hardware with GPU accelerators. The implementation of the present code on the TSUBAME2.0 supercomputer succeeded in directly resolving the fine flow structures, like bubble, spray and film of millimeter size in real-case applications. Further efforts will be devoted to improve the efficiency of the Poisson solver and to physical models, such as the wetting effects of the solid surface. More real-case applications will be conducted for product design.

References

[1] T. Yabe, T. Aoki: A Universal Solver for Hyperbolic-Equations by Cubic-Polynomial Interpolation 1. One-Dimensional Solver, Comp. Phys. Comm., Vol. 66, pp.219 (1991)

[2] T. Yabe, T. Ishikawa, P. Y. Wang, T. Aoki, Y. Kadota, F. Ikeda: A Universal Solver for Hyperbolic-Equations by Cubic-Polynomial Interpolation 2. 2-Dimensional and 3-Dimensional Solvers, Comp. Phys. Comm., Vol. 66, pp233 (1991)

[3] T. Aoki: Multi-dimensional Advection of CIP (Cubic-Interpolated Propagation) Scheme, CFD Journal, Vol. 4, pp.279 (1995)

[4] A. Ikebata, Y. Muraoka, F. Xiao: Multiphase Fluid Simulations on a Multiple GPGPU PC Using Unsplit Time Integration VSIAM3, Progress in Nuclear Science and Technology, Vol.2, pp.491 (2011)

[5] T. Yabe, R. Tanaka, T Nakamura, F. Xiao: Exactly Conservative Semi-Lagrangian Scheme (CIP-CSL) in One Dimension, Mon. Wea. Rev., Vol. 129, pp.332 (2001)

[6] F. Xiao, A. Ikebata, T. Hasegawa: Numerical Simulations of Free-interface Fluids by a Multi-integrated Moment Method, Computers and Structures, Vol. 83, pp.409 (2005)

[7] A. Ikebata, F. Xiao: Development of Conservative Front Capturing Scheme and Applications to Multi-fluid Simulations, Proc. Annual Conference of Japan Society of Mechanical Engineering, 3, pp.301 (2002) (in Japanese).

[8] F. Xiao: A Computational Model for Suspended Large Rigid Body in 3D Unsteady Viscous Flow, J. Comp. Phys., Vol. 155, pp.348 (1999)

[9] W.J. Rider, D.B. Kothe: Reconstructing Volume Tracking, J. Comp. Phys., Vol. 141, pp.112 (1998)

[10] B.V. Leer: Towards the Ultimate Conservative Difference Scheme Part V : A Second Order Sequel to Godunov's Method, J. Comp. Phys., Vol. 32, pp.101 (1979)

A Hybrid Quantum-Classical Simulation study on the Li Diffusion in Li-Graphite Intercalation Compounds

Nobuko Ohba* Shuji Ogata** Takahisa Kouno*** Ryoji Asahi*
* Toyota Central R&D Labs., Inc.   ** Nagoya Institute of Technology   *** Institute for Solid State Physics; The University of Tokyo

The Li diffusion process in the Li-graphite intercalation compound (Li-GIC) is investigated by the hybrid quantum (QM)-classical (CL) simulation. The region that includes the inserted Li and neighboring C atoms is treated with electronic state by the QM calculation and then embedded into the CL system of graphite described with an empirical interatomic potential model. A series of the hybrid QM-CL simulation runs on the dynamics of a Li-ion in the Li-GIC at constant temperature for various values of the averaged inter-layer distance of graphite is performed. We thereby find that the Li diffusivity is suppressed substantially when the inter-layer distance is compressed by a few percent from the equilibrium value. On the other hand, in the equilibrium and stretched cases, the diffusive motion of the Li-ion is composed of ballistic and hopping modes. It is found that the Li-ion existing around the middle of the upper and lower C-layers diffuses fast. Therefore as a result of trying to control the Li position between neighboring two layers of graphite using an external electric field, we find that in-plane diffusivity of the Li-ion is enhanced by suitable amplitude and frequency of the electric field perpendicular to the C-layers.

Introduction
1

The graphite can form various intercalation compounds by incorporating atoms (ions) and small molecules between the carbon (C) layers. Among these, the Li-graphite intercalation compound (Li-GIC) is put to practical use as a negative electrode of the Li-ion rechargeable battery. Among the key processes, the transport process of the Li-ions in the graphite layers is related directly to the power performance of the Li-ion batteries. With the Li insertion process, the Li-ion creates a long-ranged stress field around itself by expanding the inter-layer distance of the graphite by approximately 10%. To take into account such a long-ranged stress field in the first-principles simulation of the Li diffusion, the hybrid quantum (QM)-classical (CL) simulation code is developed.

For understanding the stress dependence of the Li diffusivity in the Li-GIC, we firstly perform a series of the hybrid QM-CL simulation runs for the dynamics of a single Li-ion in the graphite at temperature of 423 K for various values of the averaged inter-layer distance. In the hybrid QM-CL scheme, the reaction region where the electronic structure should be treated by a highly accurate calculation technique such as the density functional theory (DFT), is embedded in a CL system of atoms described with an empirical interaction model. It is expected that we can simulate the realistic large-scale system to reproduce the physical phenomenon of our interest by using the hybrid method. Remarkable merits of using the hybrid QM-CL method for the present simulation of the Li-ion in the Li-GIC are the following.

(i) The hybrid method can investigate the diffusion process of the Li-GIC with the influence of surrounding C atoms taken into consideration at a reasonable computational cost. On the other hand, the CL molecular dynamics (MD) method cannot describe generally the chemical reactions such as the charge transfer between the Li and C atoms. Also the first-principles MD method that uses the DFT for electronic structure calculation cannot treat a large-scale graphite system required to study the migration of the Li-ion.

(ii) The dispersion forces for the inter-layer interaction of the graphite can be incorporated easily through the CL interatomic potential model in the hybrid QM-CL method. Remember that the dispersion force cannot be taken into consideration in the conventional DFT method.

(iii) It is not necessary to construct an empirical interatomic potential between the Li and C atoms. If we succeed to construct the proper interatomic potential between the Li and C, we can simulate the Li diffusion in the Li-GIC by the CL-MD method. However, as we will show in § 3.2, the activation energy for the Li diffusion is quite small. It is not easy to construct a precise potential between the Li and C atoms for our purposes.

Moreover, we will analyze the relation between the vertical position and diffusivity of the Li-ion in graphite. Motivated by the results of the present analyses, we will perform additional hybrid simulations to demonstrate enhanced thermal diffusivity of the Li-ion by applying various settings of the amplitude and frequency of alternating electric fields perpendicular to C-layers.

Method

2

2.1 Buffered cluster method

In the hybrid QM-CL simulation method, a cluster of atoms is selected from the total system as the QM region. Artificial dangling bonds therefore form at the QM-CL boundary. Possible influence of the dangling bonds on the electronic states and the atomic forces should be minimized. The link-atom method that uses the hydrogen atoms for termination of the dangling bonds is often adopted to couple the QM and CL regions. Depending on the selection of the QM region, however, using the link atom method results in significant relaxation of the artificial surface of the QM region and unwanted deformation of the whole system from the original configuration. We therefore adopt the buffered cluster method (BCM) [1], which requires no link-atom and is insensitive to the selection of the QM region. To use the BCM, we put additional atoms of either H or C (i.e., constituent species), called the buffer atoms, at the QM-CL boundaries to terminate the dangling bonds. The positions of the buffer atoms are determined so as to minimize the potential energy of the corresponding cluster in CL calculation under the constraint of fixed the positions of atoms in the QM region. Note that the positions of the buffer atoms are not relaxed in the QM calculation. Thereby artificial surface relaxation of the QM region is suppressed in the BCM.

2.2 QM calculation

For the QM calculation in the hybrid QM-CL simulation, we use the real-space grid based DFT (RGDFT) method in which the Laplacian operations in the Kohn-Sham and Poisson equations are evaluated with the finite difference method. The RGDFT is well-suited to the present setting of the free boundary condition in the QM calculation and is highly parallelizable. The details of the algorithm were described in Refs. [2-4]. The Troullier-Martin-type normconserving pseudopotentials [5] are used to describe the interaction of the valence electrons and nuclei (ions). The generalized gradient approximation formula with partial core correction [6] introduced by Perdew, Burke, and Ernzerhof [7] is adopted to the exchange-correlation energy term. The Kohn-Sham orbitals and Hartree field are represented on the uniform Cartesian mesh points. The fourth-order finite-difference method is used for the Laplacian operation [8].

For parallel computation, those data on the mesh points are divided into domains to be stored in the compute nodes. The multi-grid method [9] is employed for acceleration of the convergence of the long-wavelength components of the data on the mesh points. The grid spacing $h=0.45$a.u.(1 a.u. ≈ 0.5292 Å), which corresponds to the cutoff energy (π/h)^2 $\sim$ 49Ry(1Ry = 13.6 eV) in the plane waves DFT method. In addition, the smaller grid spacing of $h/3$ is used only around the atoms.

For the QM region with buffer atoms under the external electric field E, we consider the following Kohn-Sham equation in the DFT:

$$\left[-\frac{\Delta}{2} + v_{eff} + E \cdot r \right] \psi_i = \varepsilon_i \psi_i \qquad (1)$$

with an eigen orbital and energy of ψ_i and ε_i, respectively (the atomic unit is used). Here, v_{eff} is the effective potential energy for an electron at r without the external electric field. Charge neutrality is assumed in the calculation. The force on atom-I is obtained by adding $F_I = Z_I E$ (Z_I is the ion charge) to the atomic force caused by electron-electron, electron-ion, and ion-ion interactions.

2.3 CL calculation

In the hybrid QM-CL simulation method, the CL-MD calculation is performed for the CL region, that is, the whole system minus the QM region. The velocity Verlet algorithm is used to integrate the Newton's equations of motion for all the atoms. The Brenner's interatomic potential [10] is adopted for the C atoms of the graphite. We employ the parameter values listed in Table I in Ref. [10] except for the equilibrium distance. The equilibrium distance is set to 1.33116Å so that the calculated equilibrium lattice constant of the graphite becomes equal to the one calculated with the QM calculation, which is slightly longer than that in Ref. [10]. Such a fine tuning of the parameters in the CL potential is necessary in order not to create artificial stress at the QM-CL boundary in the hybrid QM-CL simulation method.

In the Brenner-type potential, the cut-off distance of the interaction is 2.0Å. It means that only the interaction between the nearest neighbor atoms belonging to the same layer is considered. To take into account the inter-layer interaction, we construct the interatomic potential model V_{vdw} [11] based the Lennard-Jones potential for the dispersion (or the van der Waals) forces for C atoms in different layers to add it to the CL potential.

2.4 Calculation model

The simulation system is composed of 3072 C atoms and a single Li-ion under the periodic boundary condition as shown in Fig.1. The graphite assumes the AB sequence since we are interested in the situation of low Li-density. The x- and y-axes are set along

the layer, while the z-axis perpendicular to the layer. The hybrid QM-CL simulation at T=0 K gives the simulation system of L_x =34.44Å, L_y = 29.83Å, and L_z = 26.97Å as the equilibrium values. Since the thermal expansion along the layer is quite small, we use the same values of (L_x, L_y) at finite temperatures also. On the other hand, the thermal expansion along the z-axis is substantial. It is provided that the coefficient of linear thermal expansion of the pure graphite in z-direction is 6.7×10^{-5} K^{-1} by the separate CL-MD simulation with the present CL potential. We assume that the same expansion coefficient can be applied to the present system since the Li density is too small to affect the system size. Therefore, multiplying the linear expansion factor for 423 K to L_z= 26.97Å for T = 0, we find the equilibrium value of L_z = 27.74Å for T = 423 K. We investigate the Li diffusion process when changes in L_z the original value of 27.74Å are -3.9, -1.7% (compressed) , 0.6% (equilibrium) and 2.9% (stretched).
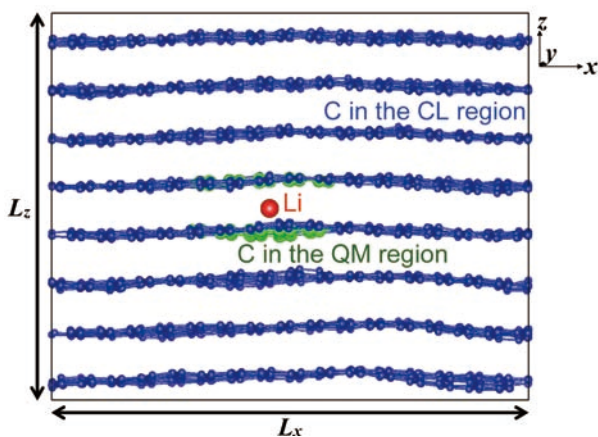

Figure 1   The side (x−y) view of the total simulation system. The large red and medium green spheres are respectively the Li and C atoms in the QM region. The small blue spheres are the C atoms in the CL region.

3 Stress dependence of the diffusivity of the Li in graphite

3.1 Li diffusion in changing interlayer space of graphite

The trajectory of the Li-ion during 10 ps in each run is plotted in Fig.2; the initial and final positions of the Li ion are depicted with the open arrow and the large red sphere, respectively. The green spheres are the C atoms in the QM region. When the graphite layers assume the equilibrium distance or stretched one, the Li ion migrates over a wide area. In the equilibrium and stretched cases (0.6 % and 2.9 %) in Fig.2, we observe both hopping and ballistic modes of the Li ion motion. In the hopping mode, the Li ion moves to avoid the places at which two C atoms belonging to different layers assume the same x-y positions (see, Fig.4). However, as remarked in Fig.2 with black arrows, we find the ion in the ballistic mode can pass through such a place. Detailed analyses of the ballistic-motion events show that the inter-layer distances at near places of the Li-ion toward the direction of its motion are always larger than 3.85Å. We, in fact, find that the thermal fluctuation produces such a local stretching frequently at various places in those simulation cases. On the other hand, in the compressed case the Li-ion diffuses in the hopping mode only and appears to be confined in the deformed layers (i.e., the cage effect).

Figure 3 shows the mean square displacements (MSD) of the Li-ion as functions of time in the four cases (-3.9% ,-1.7% , 0.6% , and 2.9% changes of L_z) at T = 423 K. Since there exists only a single Li-ion in the system, we shift the time origin of the MSD by every 0.01ps to increase the number of data samples for better statistics. The total simulation time is 12ps for Li each run; the time step is 1.0 fs. The curves in Fig.3 are not linear enough to estimate the diffusion coefficients at long times. However, characteristic dependence of the Li diffusivity on the change of L_z is observed as follows. The MSD's in the equilibrium (0.6%) and stretched (2.9%) cases are larger than that in the compressed (-1.7 % and -3.9 %) cases. However, the long-time diffusion in 2.9 % of stretched case tends to become slightly slow. This is because the Li-ion is trapped near the upper or lower graphite layer and the details will be provided later. In a compressed case, the clear change of the MSD from the linear to saturation behavior is observed. The mechanism of the saturation behavior is explained in terms of the cage effect.
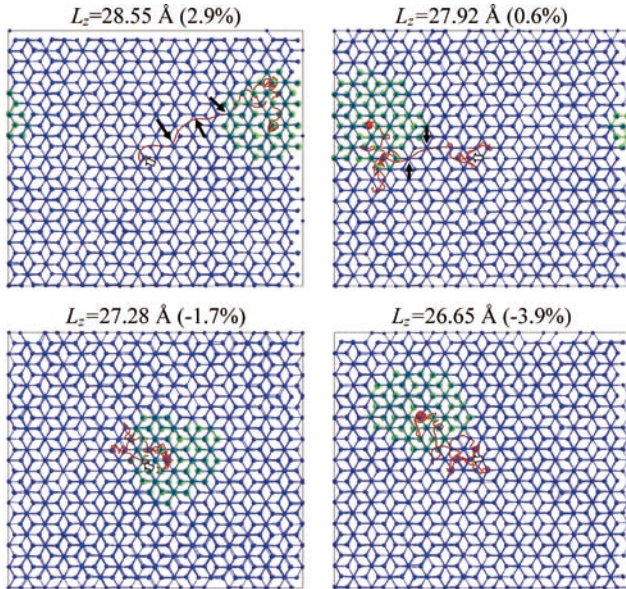
Figure 2 The trajectory of the Li ion during 10 ps viewed from z-direction, obtained in the hybrid QM-CL simulation. The four cases of the change of L_z are considered. The initial and final position of the Li ion is depicted by the open arrow and the large red sphere, respectively. The green spheres are the C atoms in the QM region. The black arrows depict the places where the Li ion passes through the places at which two C atoms belonging to different layers assume the same x- y positions.
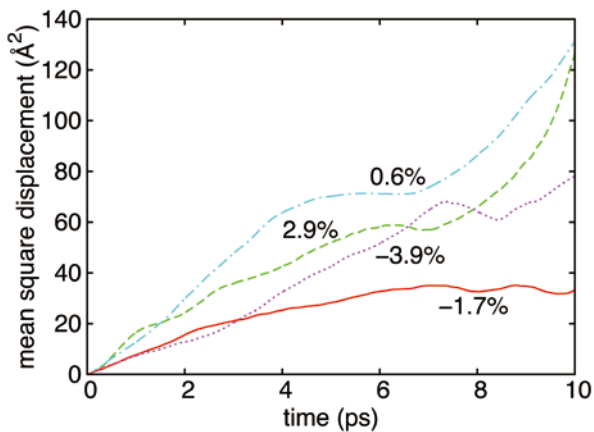
Figure 3 The mean square displacements of the Li-ion as functions of time in the hybrid QM-CL simulation at *423* K for the compressed (*-3.9*% and *-1.7*%), equilibrium (*0.6*%) and stretched (*2.9*%) values of L_z.
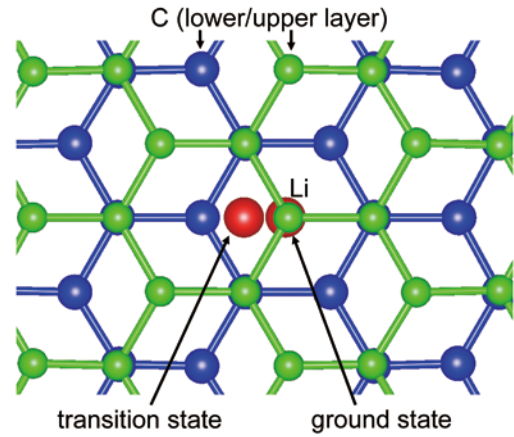
Figure 4 The Li ion at the ground and transition states in the hopping diffusion in the graphite. The Li ion is sandwiched by two C-layers.

3.2 Activation energy

In order to understand the mechanisms of the Li diffusivity, the activation energy for the hopping diffusion of the Li ion is evaluated using the hybrid QM-CL simulation method. Figure 4 depicts the positions of the Li ion in the ground state (GS) and the transition state (TS). The activation energy, which is calculated by subtracting the energy in the GS from that in TS, in each case of the L_z change is plotted in Fig.5. The activation energy obtained from the total energy, i.e., the filled sphere in Fig.5, includes both contributions of the QM and CL regions. We find that the activation energy is quite small, less than 0.07eV, irrespective of L_z. Therefore, the Li ion can diffuse easily by the thermal fluctuation. As the inter-layer distance becomes shorter, the activation energy estimated from the total energy increases substantially, which supports our finding of suppressed diffusivity by compression. The contribution of the QM region (i.e., around the Li ion) to the activation energy changes little when the system is compressed or stretched. On the other hand, the contribution of the CL region (far from the Li ion) increases as the system is compressed, which means that the distortion of the C atoms far from the Li ion affects the activation energy.

To analyze possible error in the activation energy, we calculate the energy with a different method in a similar setting. We use the projector augmented wave method for the DFT calculation implemented in the VASP code [12], which is expected to have higher accuracy since the core electrons are treated also in addition to the valence electrons. We prepare the supercell, 3 ×3×2 of the unit cell, of the graphite in the AB-sequence. Then a single Li atom is inserted. Hence the total system contains *72* C

atoms and 1 Li atom. The calculated results by the VASP are listed in Table 1 for both GS and TS. The activation energy evaluated from the electronic energy is 0.09 eV, which is the same order obtained by the hybrid QM-CL simulation method at zero strain. Considering the difference in the target system used in the two methods, we state that no substantial difference in the activation energy exists between the two results. In addition we calculate the activation free-energy using the phonon package MedeA[13]. Relatively large contribution of the phonon entropy $T\Delta S = -0.14$ eV is found at 400 K. Finally the difference in the Gibbs free-energy between the GS and TS becomes 0.04 eV.
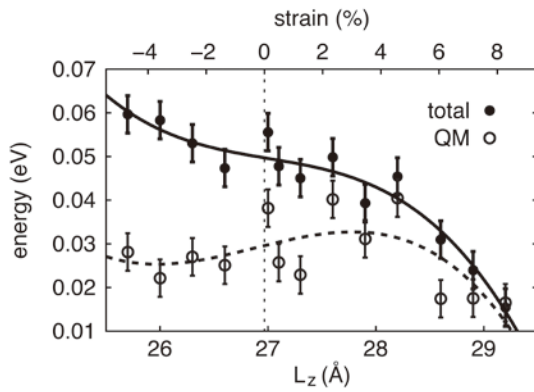
Figure 5 The activation energy for the hopping diffusion of the Li ion in the graphite at T=0K calculated using the hybrid QM-CL simulation method. The filled circles with the solid line represent the data evaluated using the total energy. The open circles with the dashed line represent the data using the energy of the QM region only. The strain corresponds to the variation of L_z from the equilibrium distance of 26.97Å at 0K. The error bars indicate the estimated overall errors relating to the convergence fluctuation in the real-space DFT method.

|	E_{ele} (eV)	pV (eV)	E_{vib}^{400K} (eV)	S_{vib}^{400K} (eV/K)	G^{400K} (eV)
GS	−7.94	2.79	13.88	0.0063	6.22
TS	−7.85	2.74	13.75	0.0059	6.26
Δ (TS-GS)	0.09	−0.06	−0.13	−0.00036	0.04

Table 1 The results of various quantities at the ground state (GS) and transition state (TS) calculated using the VASP code. The E_{ele}, E_{vib}^{400K}, S_{vib}^{400K}, and $G^{400K} = E_{ele} + E_{vib}^{400K} + pV - TS_{vib}^{400K}$ are the electronic energy at T=0K, the vibrational energy including the zero-point energy, the phonon entropy, and the Gibbs free-energy at T=400 K, respectively. The electronic energy is measured in reference to the standard states of the atomic elements.

Enhancement of Li diffusion by external electric field

4

4.1 The relation between the vertical position and diffusion behavior of Li at E=0

Firstly, we analyze the relation between the vertical position and diffusion behavior of the Li ion observed in the hybrid simulation run with a zero electric field, i.e., *E=0*. The stretched case (*2.9 % , L_z=28.55*Å) in which the Li-ion diffuses well is adopted. Figure 6 (middle) shows the time evolutions of the distances d_u and d_l between the Li ion and the center-of-mass positions of QM-region C atoms in the upper and lower layers, respectively. The time evolutions of absolute values of Li displacement in the *x-, y-,* and *z*-directions $|(R_{Li(t)} − R_{Li(0)})_{x,y,z}|$ are shown in Fig.6 (bottom). In most of the period of t=0 to 1 ps, d_l is shorter than d_u, which means that the Li-ion is trapped near the lower layer. During the period, the Li-ion hardly diffuses, as shown in Fig.6 (bottom). In the following period of t=1.0 to 1.2 ps, on the other hand, d_l and d_u are nearly equal and the Li diffusivity is relatedly high. Such a relation between d_l, d_u and the in-plane displacements of the Li-ion can also be seen at approximately t=1.6 ps and 4.2 ps in Fig.6. We may state that Li diffusivity is enhanced when the Li-ion escapes from one of the two stable vertical sites to move around the middle of the upper and lower layers where a resisting force on the Li ion for the perpendicular (*x* or *y*) motion is relatively weak.
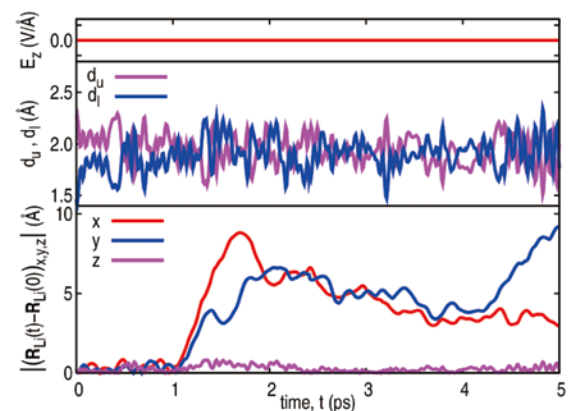
Figure 6 Diffusion behavior of Li-ion in graphite at T=*423* K with zero external electric field, observed in hybrid QM-CL simulation run. The time evolutions of the external electric field, d_u and d_l, and the absolute values of the Li displacements in three directions are depicted in top, middle, and bottom panels, respectively.

## 4.2 Li diffusion in applying external electric field

Motivated by the finding stated above, we think of increasing the mean probability of the Li residence around the middle of the upper and lower C-layers to enhance the diffusivity of the Li-ion in graphite by applying an alternating electric field perpendicular to C-layers.

Figure 7 shows the MSD of the Li-ion as functions of time $\langle |(R_{Li(t)} - R_{Li(0)})|^2 \rangle$ obtained in the hybrid QM-CL simulation runs at T = 423 K with electric field amplitudes $E^{amp}_z =0.0, 0.14$, and 0.43 V/Å and frequencies $f =0.4, 0.8$, and 1.7 THz. For better statistics, the time origins are set every 10 fs in a simulation run with a total of 5 ps. As E^{amp}_z increases with $f =0.4$THz, the Li diffusivity gets lower. This is because the Li-ion experiences a force to stay around one of the two stable vertical sites exerted by the vertical electric fields at such a relatively low frequency. From the Fig.5, the activation energy for the hopping diffusion of the Li ion is estimated as about 0.04 eV for the present system size of $L_z = 28.55$Å. Since the vertical distance between the stable vertical site and the transition state site is about 0.2Å, $E^{amp;thres}_z = 0.04/0.2 = 0.2$ V/Å may be the threshold value for such a vertical transition of the Li-ion to occur without the thermal energy. The Li-ion is expected to escape quickly from one of the two stable vertical sites following the time evolution of the electric field if $E^{amp}_z > E^{amp;thres}_z$.

We therefore analyze the f dependence of $\langle |(R_{Li(t)} - R_{Li(0)})_{x,y,z}|^2 \rangle$ for $E^{amp}_z= 0.43$ V/Å, which is larger than $E^{amp;thres}_z$. As shown in Fig. 7, the Li diffusivity at $f = 0.8$ THz is similar to that at $f = 0.4$ THz and that the Li diffusivity at $f = 1.7$ THz is remarkably high. The time evolutions of the Li-C distances d_u and d_l for $E^{amp}_z = 0.43$ V/Å at $f = 0.4$ and 1.7THz are shown in Fig.8. At $f = 0.4$ THz, the vertical position of the Li ion is high (low) when the electric field directs upward (downward) as seen in Fig.8(a). Since the Li-ion hardly diffuses when it stays at one of the two stable vertical sites, the effective diffusivity becomes low at such a low frequency. At a high frequency of $f = 1.7$ THz, the Li-ion changes its vertical position in a chaotic manner with the large and alternating vertical forces on it owing to the external electric field, as shown in Fig. 8(b). It appears that the vertical motion of the Li-ion cannot catch up with such a fast change in the direction of the external electric field. In other words, the Li ion experiences a retarding force from the external electric field before arriving at a stable vertical site. The Li ion therefore increases its probability of residing around the middle of the upper and lower layers, resulting in a significant enhancement of Li diffusivity.

The valence-electron density distribution in the QM region applied the electric field which of amplitude is 0.43 V/Å statically is shown in Fig.9. If the amplitude of electric field is too large, valence-electron cloud have possibilities to greatly slip off from the atomic nucleus position. Present electric field amplitude of 0.43 V/Å is a considerably strong, but the electronic distribution remains around the carbon atom of the QM region.

No experimental report exists about the vibrational frequency peak of Li-GIC in the range of $1 \sim 2$ THz. For graphite, the low-frequency mode of $E_{2g(1)}$ is observed at 1.26 THz in the Raman measurement [14]. If the oscillation frequency of the external electric field is tuned to the mode, it is likely that the vertical vibration of the layers in graphite enhances Li diffusivity further by increasing the probability of the Li residence around the middle of the upper and lower layers. We note that no such vibration of the layers is observed in the present simulation runs. Technologies for generating high-intensity radiation in the terahertz range have been advancing rapidly in recent years, for example, using the gyrotron system[15]. Experiments to demonstrate our present prediction of enhanced Li diffusivity in graphite by using an alternating vertical electric field should be possible in the near future.
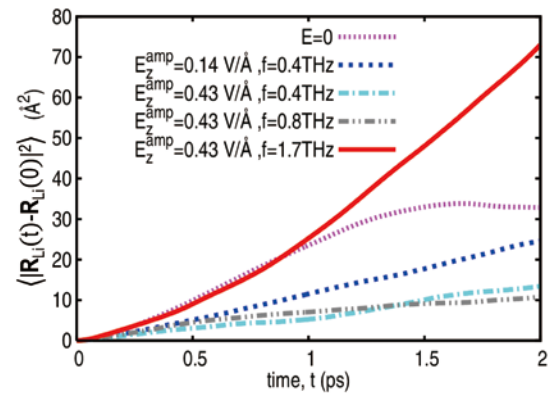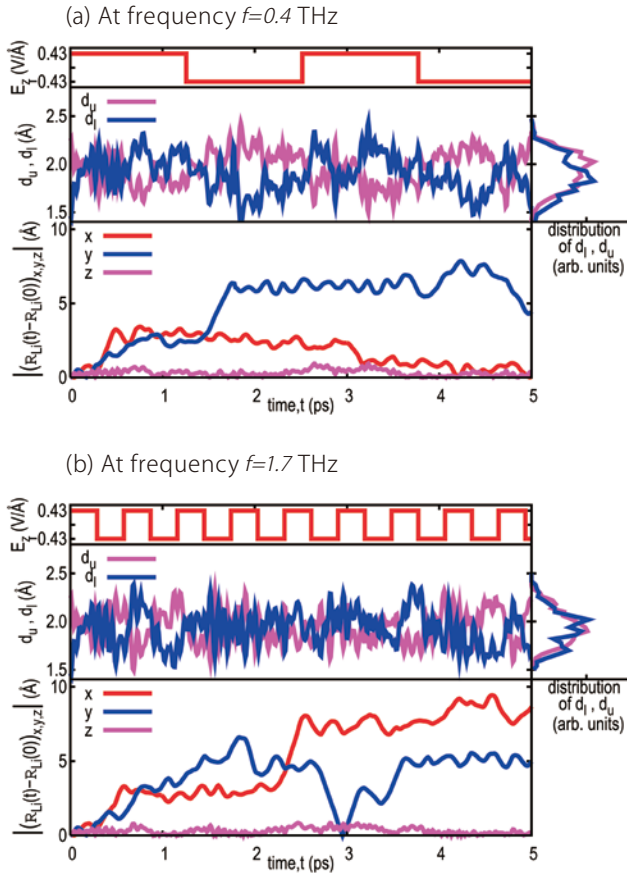

Figure 7 Time evolutions of mean squared displacements of Li ion obtained in hybrid QM-CL simulation runs at T = 423 K with various external electric fields. For better statistics, the time origins are set every 10 fs in a total simulation period of 5 ps.

(a) At frequency *f=0.4* THz
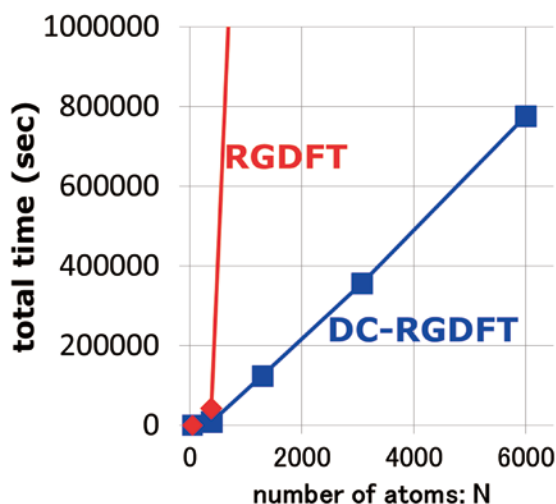

(b) At frequency *f=1.7* THz

Figure 8 Same as Fig.6, but with the external electric field amplitude $E_z=0.43$V/Å . The right side graphs of the middle panel show probability distributions of d_u and d_l, which are obtained by taking average of 5 ps.

Figure 9 The valence-electron density on a y-plane in the QM region applied the electric field which amplitude of *0.43* V/Å. The black sphere is the Li ion, while the gray spheres the C atoms. The density less than *0.001* a.u.$^{-3}$ is omitted.

Summary

5

We have applied the hybrid QM-CL simulation code to analyze the stress dependence of the diffusivity of a single Li-ion in the graphite at T=*423* K by changing the averaged inter-layer distance (by plus and minus a few percent). Thereby we have found that the Li diffusivity is suppressed significantly in the compressed case, while in the stretched case, the Li-ion motion has shown both hopping and ballistic modes. On the other hand, in the compressed case, the Li ion has diffused through the hopping mode only and has been found to be confined in a relatively small area at longer times; its mechanism has been explained in terms of the cage effect. From our findings about the stress-dependence of the Li diffusivity in the graphite, we think a possible mechanism for the drastic lowering of the Li diffusivity at particular densities of Li observed experimentally in the Li-GIC.

We have found that the in-plane diffusivity of the Li-ion at T = *423* K is enhanced significantly by the electric field perpendicular to the C-layers if the amplitude $E^{amp}_z > 0.2$ V/Å and the frequency *f* is as high as *1.7* THz. The mechanisms of the enhanced diffusivity have been explained in terms of the increased probability of the Li residence around the middle of the upper and lower layers, resulting in a weak interaction between the Li ion and the graphite layer.

In the present simulation, the real-space grid based DFT (RGDFT) code suited to the parallel computer has been adopted for the QM calculation in hybrid simulation. From the viewpoint of computational cost, the RGDFT cannot handle large-scale system including many atoms, because its computational time increases in proportion to N^3 (N: the number of atoms including in the system). Therefore we have developed the novel order-N Divide-and-Conquer (DC) type RGDFT code, in which we divide the target system into several domains[16]. Figure 10 shows a benchmark test of the DC-RGDFT code on TSUBAME2.0 for large-scale Al cluster. Five calculations for the system including the Al atoms of 48, 384, 1296, 3072, and 6000 have been performed with dividing 1, 8, 27, 64, and 125 domains, respectively. The number of SCF iteration is fixed to 25. The computation power increases linearly with N in order to treat 4 atoms per 1 CPU-core. It is confirmed that the total calculation time using the DC-RGDFT scale linearly with N, while that of RGDFT increase proportionally with N^3. The use of DC-RGDFT for larger scale QM region in hybrid QM-CL simulation is now in
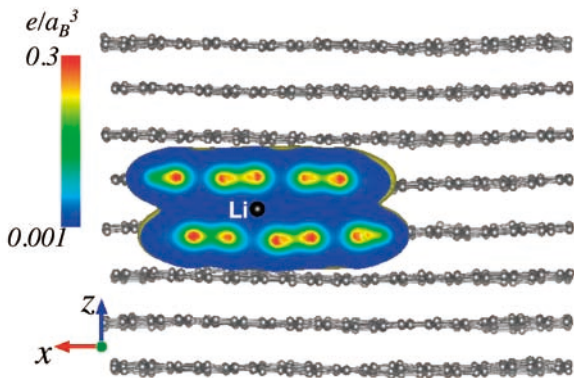
progress. We are working on the case of existing multiple Li's in the Li-GIC, and the effects the Li-Li interaction to the Li-ion dynamics will be clarified.

Figure 10 The total calculation time for Al cluster system of various numbers of atoms N by the RGDFT and DC-RGDFT method.

References

[1]   S. Ogata, Phys. Rev. B 72, 045348 (2005).

[2]   S. Ogata, E. Lidorikis, F. Shimojo, A. Nakano, P. Vashishta, and R. K. Kalia, Comput. Phys. Commun. 138, 143 (2001).

[3]   S. Ogata, F. Shimojo, R. K. Kalia, A. Nakano, and P. Vashishta, Comput. Phys. Commun. 149, 30 (2002).

[4]   F. Shimojo, T. J. Campbell, R. K. Kalia, A. Nakano, S. Ogata, P. Vashishta, and K. Tsuruta, Future Gen. Comp. Sys. 17, 279 (2000).

[5]   N. Troullier and J. L. Martins, Phy. Rev. B 43, 1993 (1991).

[6]   S. G. Louie, S. Froyen, and M. L. Cohen, Phy. Rev. B 26, 1738 (1982).

[7]   J. P. Perdew, K. Burke, and M. Ernzerhof , Phy. Rev. Lett. 77, 3865 (1996).

[8]   J. R. Chelikowsky, N. Troullier, and Y. Saad, Phys. Rev. Lett. 72, 1240 (1994).

[9]   A. Brandt, Math. Comput. 31, 333 (1977).

[10] D.W. Brenner, Phys. Rev. B 42, 9458 (1990); 46, 1948(E) (1992).

[11] N. Ohba, S. Ogata, T. Tamura, S. Yamakawa and R. Asahi, CMES-Comp. Model. Eng. 75, 247 (2011).

[12] G. Kresse and J. Furthmüller, Phys. Rev. B 54, 11169 (1996).

[13] K. Parlinski, Medea-phonon, materials design, inc., 2003, based on K. Parlinski, phonon 3.11, 2002.

[14] R. Kostic, M. Miric, T. Radic, M. Radovic, R. Gajic, and Z. V. Popovic: Acta Phys. Pol. A 116, 718 (2009).

[15] T. Saito, T. Notake, Y. Tatematsu, A. Fujii, S. Ogasawara, L. Agusu, T. Idehara, S. Kubo, T. Shimozuma, K. Tanaka, M. Nishiura, K. Kawahata, and V. N. Manuilov: J. Phys. Conf. Ser. 227, 012013 (2010).

[16] N. Ohba, S. Ogata, T. Kouno, T. Tamura and R. Kobayashi, Comput. Phys. Commun. 183, 1664 (2012).

A Large-scale Simulation on CFD in Construction Industry

Pham Van Phuc* Tsuyoshi Nozu* Hirotoshi Kikuchi* Kazuki Hibi**

* Center for Advanced Computational Engineering, Shimizu Institute of Technology   ** Numerical Flow Design CO., LTD.

Predicting the performance of computer in a CFD application is an important issue in the practical fields. In this paper, the performance of a single compute node, GPU and computing networks by year have been investigated. Large-scale simulation in massively parallel process is necessary to maximize the performance of computer at present. The usefulness of large-scale simulation in using high resolution grid in order to achieve more accuracy results in comparison with experimental results, in using small grid size to develop a more elaborate numerical model reproducing much more flexible shape of object, or to simulate a wide urban area considering the effect such as surrounding complex terrain to buildings are also discussed together.

Introduction 1

Improving the performance of supercomputers[1] at a rate of 1000 times in the last 10 years has been realized by using the modern devices such as GPU and taking advantage of high-speed and large bandwidth network with many compute nodes. However, what has been changed or should to be changed in the daily use of computer, the issue has not been discussed much in the field of manufacturing and other industries.

In the construction industry, building a safe, secure and comfortable living environment under considering the effects of surrounding environment is most important. Many problems such as estimation of wind load, tsunami load on buildings, and evaluation of thermal and wind environment around them need to be solved together. While the experimental and empirical evaluations are limited, numerical simulation is found as an effective method to solve these problems. Recently, during the wide spread of BIM (Building Information Modeling) with large-scale three-dimensional data, the numerical model itself becomes much more flexible. Simulating a large-scale model is more challenging and it comes with a high compute cost. Maximize the computational capacity of computer is a necessary and urgent issue nowadays.

In this paper, the authors try to discern the computational ability of computer system in an application of computational fluid dynamics (CFD) from a practical standpoint. Some applications are also discussed in here to mark the importance of large-scale simulation in our construction industry.

Trends in performance of computer in a CFD application 2

Understanding the computational performance of computer is important in practical applications. In order to clarify its performance, we investigate the changing by year of the performance on single compute node, on the network of computer systems, and the scale of numerical model in a practical CFD application. Because of small different performance between CFD software using the equivalent analytical methods, the open source OpenFOAM[2] is used in this study.

2.1 Performance on single compute node[3]

Fig.1 shows the increasing of the performance of computer by year on a CFD application of wind environmental analysis for an urban area with a 10 million unstructured mesh. In the figure, the vertical axis illustrates the speedup has been normalized by the computed time of one CPU core or a compute node at the year of 2006. In here, the CPU AMD Opteron in 2006 which was adopted in TSUBAME1.0, the Intel CPU Westmere-EP in 2010 which was adopted in TSUBAME2.0, the Intel CPU Xeon in 2008 and the Intel CPU SandyBridge in 2012 are considered. From 2008 onward, although the clock rate of CPU had not changed so much, the speedup of a CPU core is now still increased due to the improved width of the CPU's data bus, the latency of the memory, the cache architecture and improved floating-point arithmetic unit. But, it is difficult to improve the performance of a single CPU core on a serial application in the future because the speedup by year has increased much more slowly. In the other hand, the speedup of a compute node using full cores in a parallel computation is growing steadily at about 1.5 to 2 times each 2 years with an increase in the number of cores every year. Therefore, parallel computation in a compute node is now an important factor to maximize the computational capacity of computer. However,

the result also indicates that improving the performance of a compute node in 10 years would be less than 32 times.

Fig.2 shows the speedup of GPU to CPU core for the solvers of a pressure Poisson equation that takes a major part of the computational time in CFD[4]. Some solvers using GPU can obtain high performance in comparison with using a CPU core in the same time. Therefore, using new devices such as GPU and developing a new appropriate computational method will be an important factor in the improvement of computational performance on CFD in the future.
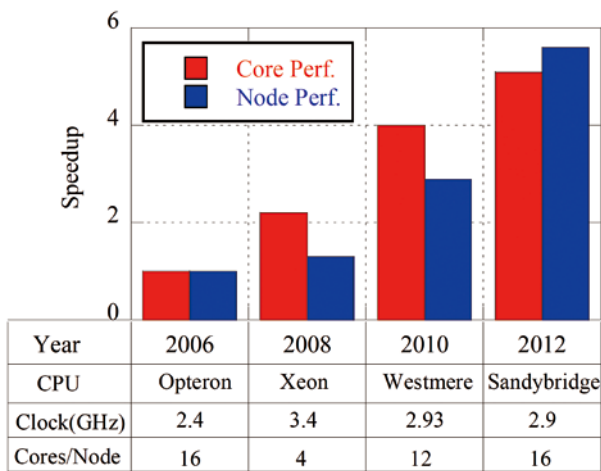
Figure 1   Increasing of CPU performance by year in a CFD application
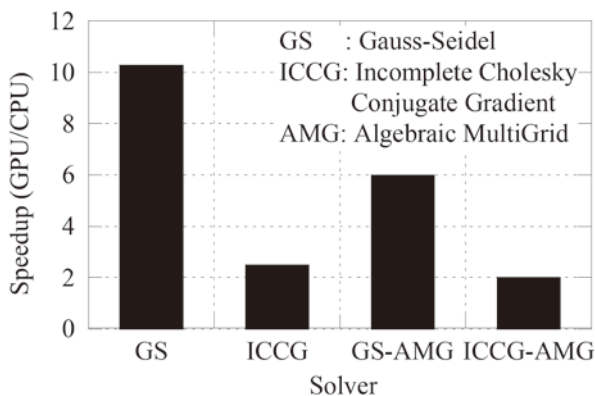
Figure 2   Speedup of GPU by CPU core in a pressure Poisson equation of a CFD application

2.2 Performance on massively parallel computation[3]

Recently, because of high performance of computer network, using many compute nodes in massively parallel computation is expected in order to improve the computational performance on CFD. Fig.3 shows the speedup by node of the Infiniband SDR network in 2006, and the Infiniband QDR network in 2010, which was adopted in TSUBAME1.0 (2 SDR lines with bandwidth of 20GBps) and TSUBAME2.0 (2 QDR lines with bandwidth of 80GBps) respectively. Two models with a 10 million and a 400 million unstructured mesh cells, are used. For the 10million mesh model, the performance is improved by network in 6 times in 4years from 2006 to 2010. The speedup also grows up much more with the increase of the number of compute nodes in the large model of 400million mesh. Therefore, large-scale model in massively parallel computation is necessary to obtain a high performance on CFD application and to maximize the capacity of computer system. Moreover, in considering the performance of a single compute node as mentioned above, it could be said that it is possible to improve the performance of computer at the rate 1000 times in 10 years on a practical CFD application.
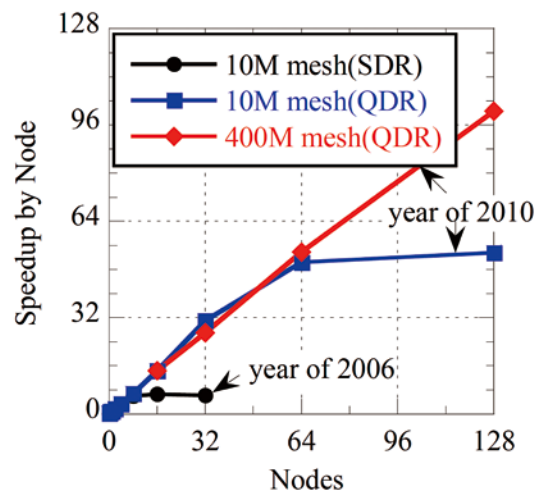

Figure 3   Speedup in different computer networks and number of meshes of a CFD model

Possibility of large-scale simulation 3

Previous chapter has discussed the computational performance of CFD focused on the single compute node, network computer hardware. It has been shown that a large-scale simulation in massively parallel computation is possible and necessary at present. In this chapter, some practical CFD applications will be discussed in order to clarify the importance of the large-scale simulation in the construction industry.

A simulation becomes larger when someone wants to use more high resolution of grid in order to improve more high precision of calculated result, to develop a more elaborate numerical model in order to reproduce a much more flexible shape of an object, or to simulate a wide-area in order to consider the effects of surrounding environment. In here, a reproducibility of an experimental wind tunnel, an elaborate mesh generation for the buildings with complex 3D shapes and an analysis of three-dimensional tsunami in wide-area using VOF method are discussed.

3.1 Reproduction of a boundary layer wind tunnel experiment[5]

Fig.4 illustrates a computational domain 30m long of a LES simulation, which was constructed to model conscientiously a boundary-layer wind tunnel measurement section including spires, fences and block roughness. The simulation is carried out for three models with 1 million mesh cells (model A), 10 million mesh cells (model B) and 100 million mesh cells (model C). Fig.5 shows the mesh sizes, the number of mesh cells and the comparison between the experimental and calculated power spectral densities of turbulence wind obtained inside the wind tunnel. The result of the model A is significantly lower in the high frequency region whose dimensionless frequency nLx/UH is less than 1. Using higher grid resolution such as model B and C, the calculated results become better. Moreover, it also shows that the numerical simulation requires approximately 100 billion mesh cells in extrapolation in order to fully reproduce the experimental results.

In addition, Fig.6 illustrates the distributions of mean and negative peak external pressure coefficients on the roofs and walls of a typical building model obtained from the pressure experiment and numerical simulation of two models with 30milliion mesh and 120million refine mesh using higher grid resolution. These coefficients are required in the assessment of wind load on claddings of buildings. The numerical simulation
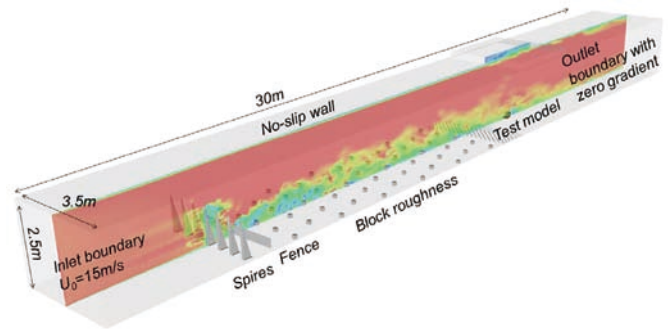

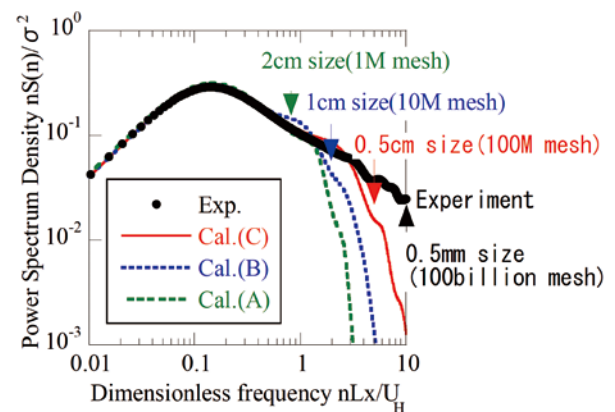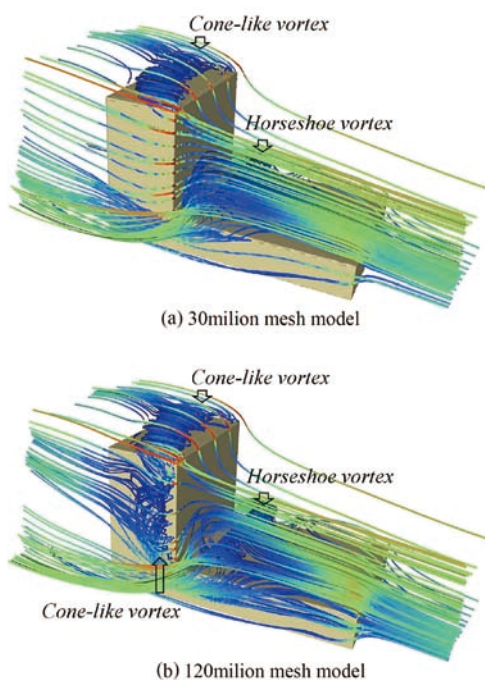**Figure 4** Computational domain of a wind tunnel

Figure 5 Power spectrum densities of wind flow

generally showed good agreement with the experimental ones for both models and identified the sensitive local pressure zones occurring on roof and wall surfaces. However, it underestimated the pressure in narrow local pressure zones. Using higher resolution mesh, the result becomes better.

Moreover, Fig.7 shows the time-averaged streamlines of the wind flow patterns around these models. For the 30million mesh model, the flow at ground level separates from the windward corner of the lower storey, descending close to the windward wall, and flows through openings beneath the upper storey. However, using 120million refine mesh model, an upward new cone-like vortex close to the side wall of the upper storey has been found together. As a result, large-scale simulation using higher grid resolution is necessary not only in an improvement of the calculation accuracy but also in the elucidation of a new mechanism in the flow field.

(a) Experimental result

(b) 30milion mesh model

(c) 120milion mesh model
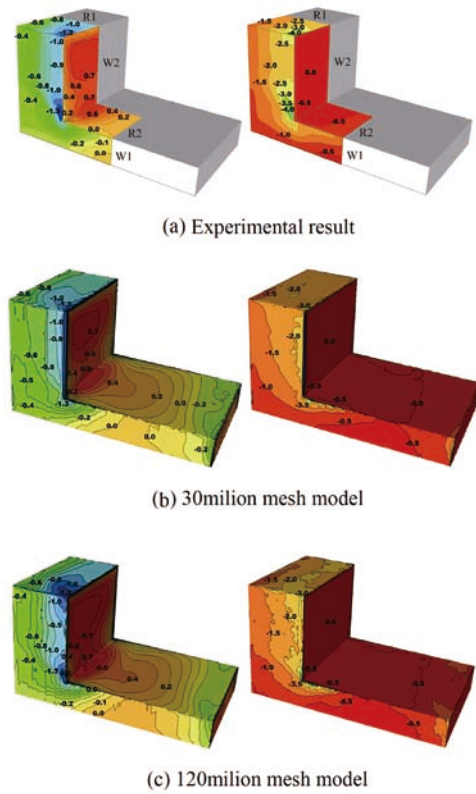
Figure 6   Pressure distributions on a building

(a) 30milion mesh model

(b) 120milion mesh model

Figure 7   Time-average streamline around building

3.2 An elaborate mesh generation for the buildings with complex 3D shapes[3]

Using advanced three-dimensional data in the construction industry is accelerated in recent years. The complex and detail 3D shapes of buildings are used increasingly in design due to many different needs. Until now, in order to obtain a mesh of a computational model of just only several million mesh, which is limited on the computer resource and its computational ability, it is necessary to use the mesh size of about several ten centimeter to meter. To generate the mesh, it is usual to clean and simplify the complex 3D shape data that suitable for the CFD. This work is often difficult and takes a lot of time depending on the details of building shapes.

It should be known that mesh generation becomes easier when mesh size is much smaller than the scale of the target model. Fig.8 shows an example of complex 3D buildings. Several centimeter of mesh size has been adopted in the mesh generation process. The mesh is generated automatically including both the indoor and outdoor sides as shown in Fg.9. Although the number of mesh reaches to 200milion cells, to be a large-scale model, building model in detail such as handrails and interior are reproduced as well.

Figure 8   Buildings with complex 3D shape

(a) Generated mesh in the outdoor side
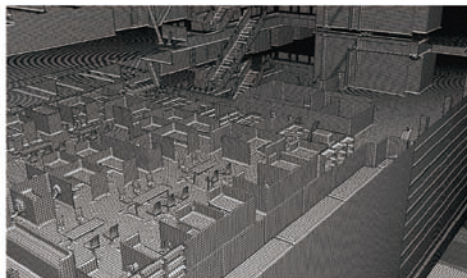
(b) Generated mesh in the indoor side

Figure 9 An example of a computational mesh

### 3.3 A large scale 3D tsunami simulation using VOF method[6]

Two-dimensional shallow water model is known as a traditional tsunami analysis that can be used to predict the inundation depth and invasion of tsunami in a wide area. However, this model could not be used directly in prediction of tsunami force acting on building or evaluation of the effects of local surrounding environment at the level of building in detail.

In the other hand, the gas-liquid two-phase flow simulation using such as VOF method[7] can reproduce the wave breaking process well, and has also been applied in some sloshing damper applications of building design. Because of the 1000 times density changing from the gas to liquid at the interface, the simulation is known as one of the most challenging theme in CFD and it takes a lot of computational time. Therefore, until now the simulation is impossible to be used in evaluation of tsunami impacting on a construction in a wide area. Taking into account the performance of computer which was discussed in the previous chapter, a large-scale simulation using VOF method is carried including a wide urban area with complex terrain of 6km*6km. Total number of mesh is approximately 50million. In order to simulate the 7 minutes time in actual phenomena, it takes 8days in the practical use of using 192CPU cores of the supercomputer TSUBAME 2.0.

As shown in Fig.10, the tsunami is reaching into the coastline. In steep mountain terrain close to the upper right portion of the coastline, tsunami inundation is obstructed. Some strong reflected wave and local concentration of high wave height distribution in narrow steep terrain and inhibitory effect of buildings and structures are confirmed. It also can be seen how the mountain and building prevent the tsunami, or how the tsunami invasion proceeds along open spaces in detail (Fig.11, 12).
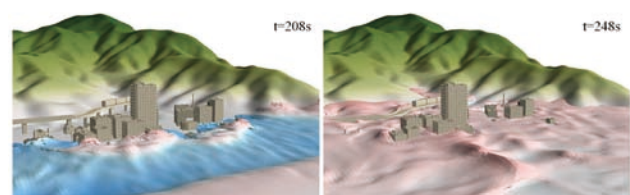
As a result, the 3D tsunami simulation using VOF method is found as an efficient method that can reproduce the behavior of the tsunami under considering the effects of such building blocks and wide urban area with complex terrain, nowadays.
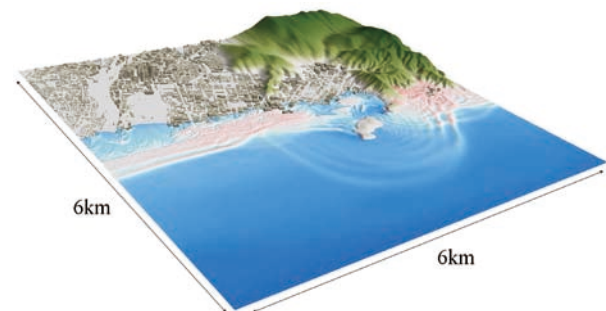
Figure 10 Computational domain and tsunami run-up in a wide urban areamesh
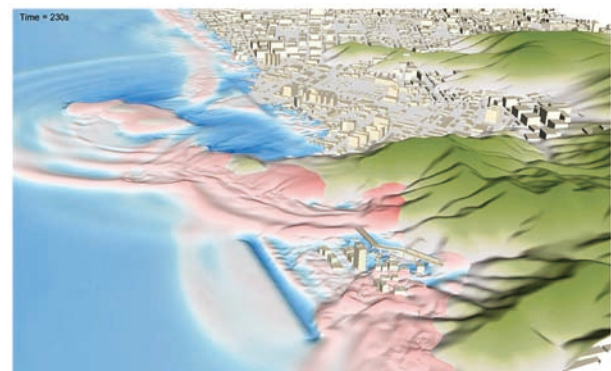
Figure 11 Tsunami run-up in complex terrain

Figure 12 Tsunami run-up in vicinity

Summary 4

From a practical standpoint, this study has shown that large-scale simulation in massively parallel computation is an important factor to maximize the performance of computer on the CFD applications of the construction industry. The large-scale simulation is also found as an useful method in the improvement of calculation accuracy using high resolution computational grid, in development a more elaborate numerical model reproducing a much more flexible shape of an object, and in a wide-area simulation of such 3D tsunami analysis using VOF method. These new calculation methods are now being established with the development of computers. Therefore, developing new evaluation methods due to the new calculation methods will be an urgent issue, nowadays.

Acknowledgements

References

[1]   Top500: http://www.top500.org/

[2]   OpenFOAM: http://www.openfoam.com/

[3]   P.V. Phuc: Computational Fluid Dynamics using An Open Source, Journal of Japan Society of Fluid Mechanics, Vol.31, pp.277-284 (2012)

[4]   P.V. Phuc, T. Nozu, H. Kikuchi, K. Hibi: A Large Parallel Computation and GPU on CFD, Proc. of the High Performance Computing Symposium, pp.75 (2011)

[5]   P.V. Phuc, T. Nozu, H. Kikuchi, K. Hibi, Y. Tamura: Local Wind Pressure Distributions on Building with a Setback obtained by Large Eddy Simulations, Proc. of the 22nd National Symposium on Wind Engineering, Vol.22, pp.359-364(2012)

[6]   P.V. Phuc, M. Hasebe, I. Takashi: A Study on Three-Dimensional Tsunami Analysis using VOF Method, Annual journal of coastal engineering, JSCE, Vol. 68, pp.71-75 (2012)

[7]   C. W. Hirt, et al.: SOLA-VOF: A solution algorithm for transient fluid flow with multiple free boundaries , Los Alamos Scientific Laboratory, pp.1-32 (1980)

Estimation of strong ground motion and damage of indoor objects during giant earthquake

Toshiyuki Masatsuki*

* Kozo Keikaku Engineering Inc.

Two programs have been ported to TSUBAME 2.0 in order to estimate the damage due to giant earthquake. One is the program for seismic wave propagation analysis and the other is for the simulation of the behavior of indoor objects. The strong ground motions due to the Tokai, Tonankai, and Nankai Earthquake have been simulated using a number of GPU. The computation time with GPU was about 10 times faster than not using GPU. The behavior of indoor objects in a warehouse has also been simulated. The computation time was about two times as fast as before.

Introduction   1

By the 2011 off the Pacific coast of Tohoku Earthquake, a wide area of northeastern Japan was devastated. It is also predicted that a wide area of Japan will suffer a great deal of damage in case the Tokai, Tonankai, and Nankai Earthquake occurs. So, it is important to estimate the earthquake damages and taking measures against the earthquake damages has become a critical issue.

Here we introduce a current situation and problems concerning earthquake damage estimation from the point of safety structural building design. And then, we show the result of industry trial use project of TSUBAME2.0 in FY2011. In the project, we have improved the practical use of the ground motion estimation and the evaluation of indoor damage due to a giant earthquake.

At first, two programs have been ported to TSUBAME2.0 in the trial use project. One is the program for seismic wave propagation analysis and the other is for the simulation of the behavior of indoor objects. Second, the strong ground motions due to the Tokai, Tonankai, and Nankai Earthquake have been simulated and the behavior of indoor objects in a warehouse has also been simulated.

Current situation of earthquake damage estimation   2

First of all, we introduce a current situation and problems about earthquake damage estimation in terms of safety structural building design.

Seismic ground motion intensity is apparently critical factor for the safety of building. There are various approaches to evaluate the strong ground motions. For now, a simple method is mainly used[ex.[1]] due to the limitations of time and cost. Seismic wave propagation analysis is also one of the evaluation methods. This method enables to simulate the more realistic seismic ground motions, especially long period ground motions, than simple methods. However, this method requires large amount of calculation and computation time. Thus, it is not commonly used except important structures. But, the guideline of Architectural Institute of Japan[2] recommends using more advanced methods such as seismic wave propagation analysis, so advanced methods may be used more often in the future.

Next, we show the current situation about indoor damage estimation. There is no detail guideline for overturning or dropping objects such as furniture unlike structural building design. In the past years, especially after the 2011 off the Pacific coast of Tohoku Earthquake, we have often noticed the danger and the damage of indoor objects. Many investigations have been reported[ex.[3]] and the various issues about indoor damage are discussed in some committees. It is possible to estimate realistic behavior of indoor objects using rigid body simulation considering detail information. But, such simulation is rarely used because it requires a great deal of time for accurate simulation. If the computation time is drastically shortened, indoor damage simulation would be used more often in order to discuss the countermeasures against indoor damage.

In Kozo Keikaku Engineering Inc., we have started the project to improve the practical use of the seismic wave propagation analysis in FY2009. In the first year, we have ported the program for seismic wave propagation analysis to Earth Simulator 2 using trial use project by the MEXT. In the second year, FY2010, we have optimized the program and added new functions. We have succeeded to shorten the computation time drastically. In addition, we have tried to calculate the shorter period ground motions to do more detail simulation. In FY2011, we have ported the program to TSUBAME2.0 in order to calculate with GPU, and the simulation program for the behavior of indoor objects have also been ported.

Wave propagation analysis 3

Here we describe the result of the trial use project of TSUBAME2.0 in FY2011.

First of all, we describe the overview of the program for seismic wave propagation analysis ported to TSUBAME2.0. This program calculates seismic wave propagation by 3D FDM. The program had already been able to calculate using a number of nodes with MPI. So, we mainly updated this program to calculate with GPU by each process by reference to Nakamura et al (2011)[4], who simulate seismic wave propagation using same method with GPU. The program was compiled by PGI Fortran compiler to use CUDA in Fortran. As a result, the computational speed with GPU was almost 10 times faster than using only CPU with -fastsse option (3.1 billion mesh, 100 nodes and 300 GPUs). Fig. 1. is the weak scaling performance of this program. This program scales well with the increasing number of GPUs. The bottle neck of this program is MPI communication time, so it is required to decrease communication data in order to make this program faster. If GPU global memory size becomes larger, it is able to proceed with same scale simulation with less parallel number, thus the computation time may become shorter. The largest scale simulation of this project was 12 billion subdomain size with 810GPUs using 270nodes. And its computation time was 4 hours for 77600 steps (duration time is about 232 seconds).

Next, we describe the seismic wave propagation simulation of the Tokai, Tonankai, and Nankai Earthquake. Fig.
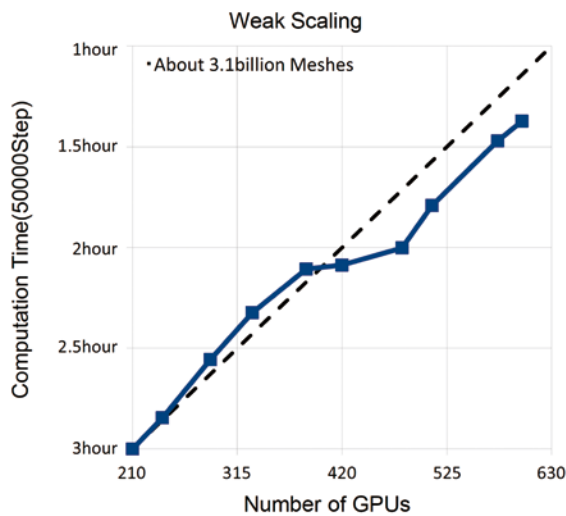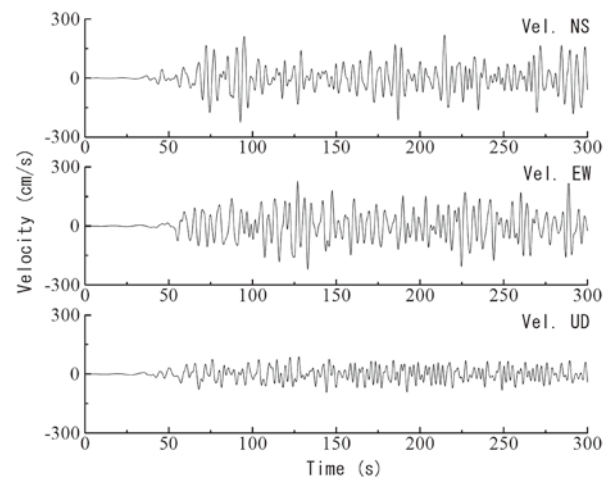

Figure 1   Weak scaling of the program for wave propagation analysis

Low Pass Filter : Period T >= 2.0sec

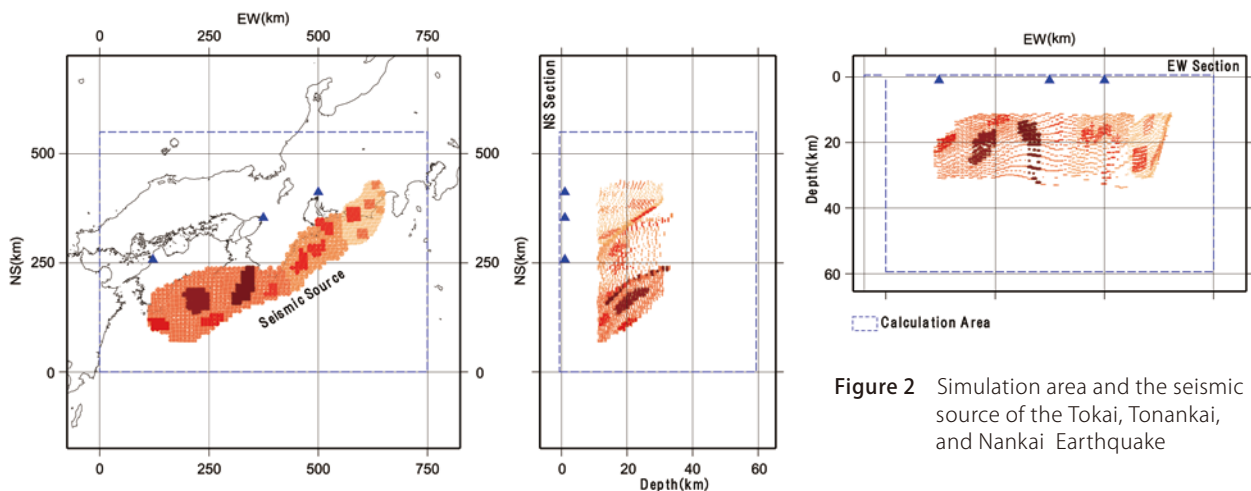**Figure 3**   Velocity Time History in Nagoya

Figure 2   Simulation area and the seismic source of the Tokai, Tonankai, and Nankai Earthquake

2. shows the simulation area and the seismic source of this earthquake. The seismic source parameters were set by reference to Central Disaster Prevention Council (2003)[5] and Yamamoto, Yoshimura et al (2012)[6]. The subdomain size is 3.1 billion (550x750x60 km), 0.2x0.2x0.2 km mesh size. The delta time is 0.006 seconds and the number of the simulation step is 50000 (duration time is 300 seconds). The computable period is more than 2 seconds. Fig. 3. shows the velocity time history on the ground surface in Nagoya. The ground shaking started at 50 seconds and continues to around 300 seconds. Fig. 4. shows the snapshot of seismic wave propagation. The contour color shows the velocity on the surface ground. The 75 seconds after the fault rapture started, the seismic wave arrives to the Osaka Plain and the Nobi Plain, and the ground shaking in the basin area continues for a long time. This is the same as observed phenomenon during an earthquake. The validation of the accuracy of this simulation is the future work.
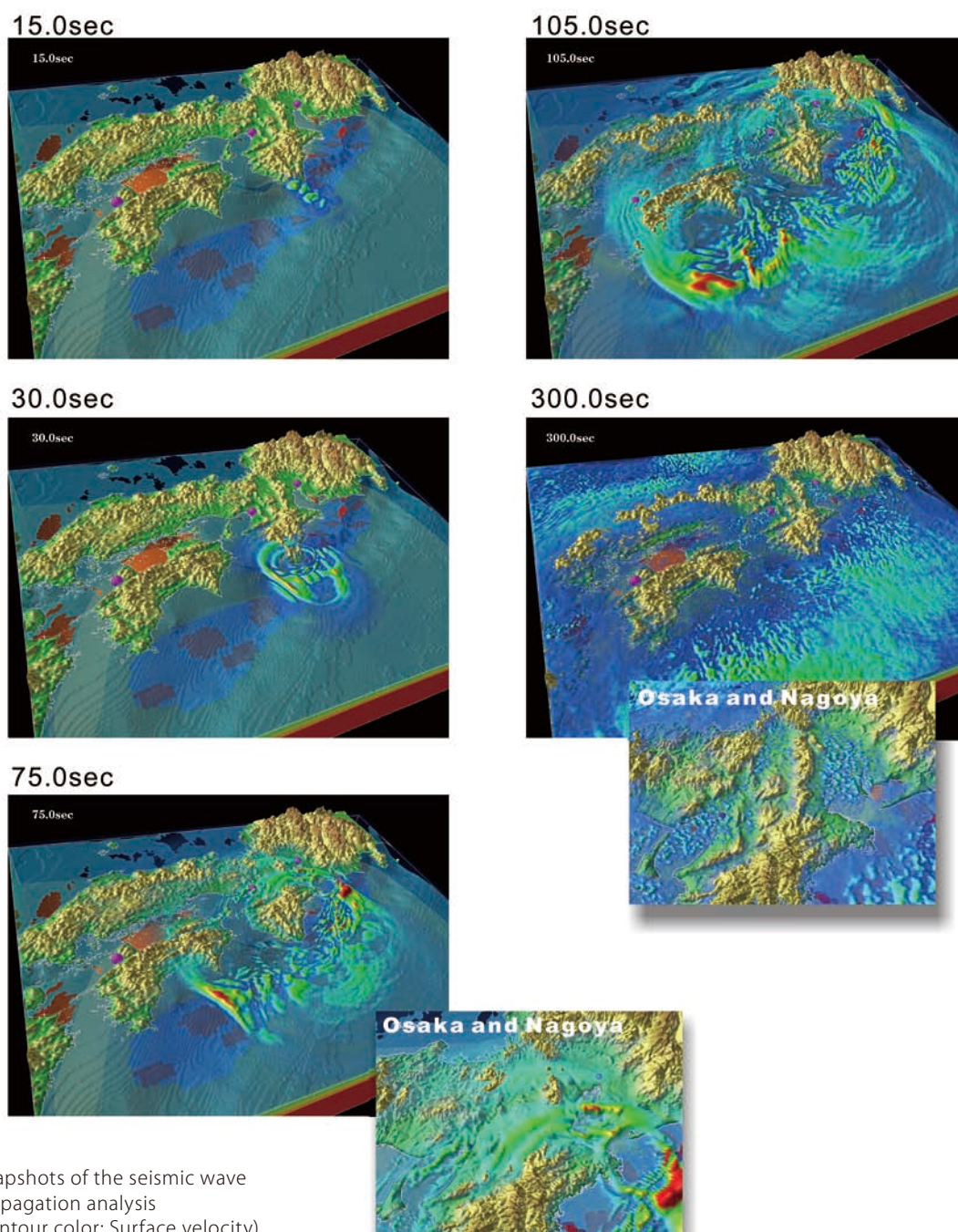
Figure 4 Snapshots of the seismic wave propagation analysis (Contour color: Surface velocity)

Indoor damage estimation   4

Now, we show the overview of the 3D rigid body dynamics simulation program for indoor damage estimation. This program can simulate the behavior of falling objects from a rack during an earthquake such as Fig. 5. Analytical Method[7],[8],[9], which treats contacts as constraints, is used in this program to calculate contact forces between colliding objects.

The brief flow of this calculation is as follows;

1. Detect collisions of rigid bodies
2. Update the constrains due to the contacts based on   the result of the collision detection
3. Calculate constraint forces including contact forces   such as a normal or friction force
4. Update velocities and positions of rigid bodies based on   equation of motion

First step porting this program to TSUBAME2.0, the program was modified to handle large scale data. Before the modification, if the number of objects were over about 1000, the simulation was stuck. After the modification, it is possible to proceed the number of objects is even more than 10000. We used Intel TBB for the parallelization and enables to calculate with multi-GPU. The process of collision detection were mainly acceralated because this process spends a big part of computation time. As the result, the computational speed of collision detection has become 3 to 4 times faster than before. In consequence, the whole computation time is about 2 times than before.

Fig. 6. shows the simulation model of indoor objects in warehouse. There are one meter square pallets showing with red line in Fig. 6., and rigid body assumed 48 jute bags are showed with white lines on the square pallets. 48 jute bags are one block and they are piled up with various directions. The whole number of jute bags was about 1400. We have confirmed the model include over 10000 rigid bodies was possible to calculate. However it took 2 weeks to calculate only several tens of seconds, and it is noticed that the calculation becomes unstable which has enormous number of objects. Therefore we could not do the simulation which has over 10000 objects.

Fig. 7. shows the result of the simulation. The wave shown in Fig. 3. is used as an input floor response. From this figure, it shows the jute bags fell down and one of the cargos is collapsed and flopped to next cargo around 76 seconds passed, which is the time for strong shaking. The result of this simulation should be validated in the future.

Figure 5   Simulation of falling objects from racks during an earthquake
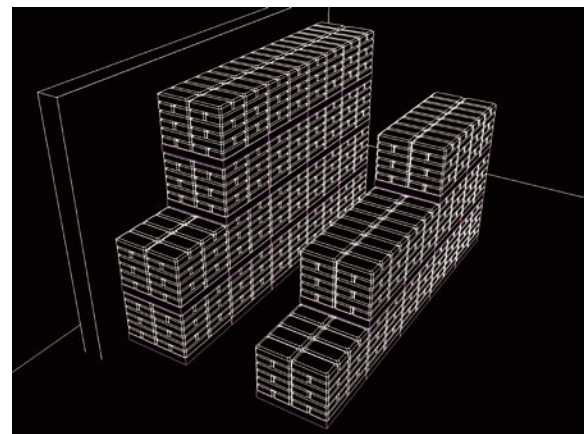
Figure 6   Simulation model of indoor objects

Conclusion   5

We have ported two programs to TSUBAME2.0. One is the program for seismic wave propagation analysis and the other is the program for simulating indoor damage due to giant earthquakes.Then, we have shortened the computation time and constructed the environment to do the simulations easier than before. We will validate the results of the simulations in the future.
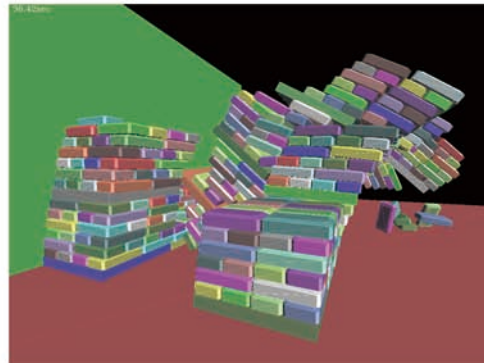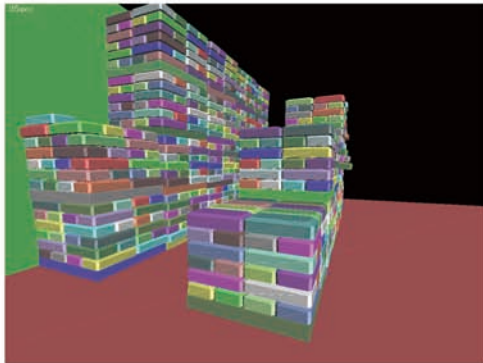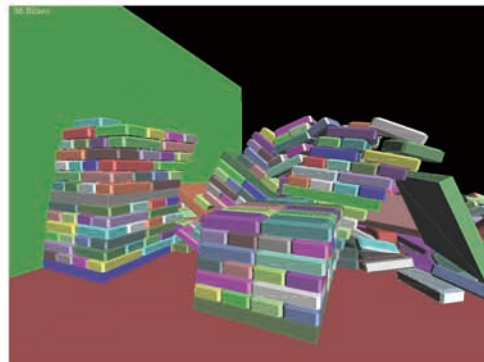
Acknowledgements

40.0sec
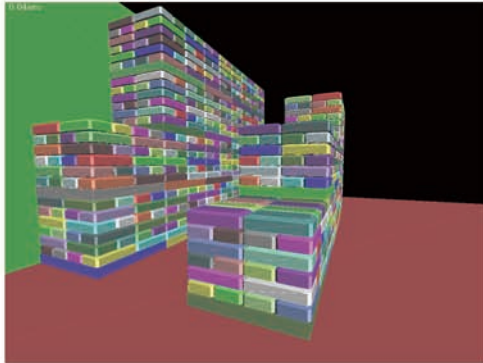
75.0sec
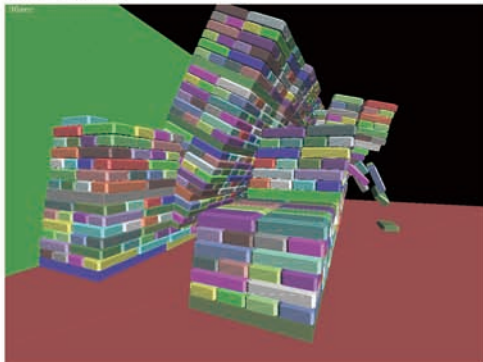
76.0sec

76.4sec

76.8sec

Figure 7   Snapshots of the simulation of indoor objects in ware house

References

[1] S. Midorikawa and H. Kobayashi: On estimation of strong earthquake motions with regard to fault rupture, Transactions of the Architectural Institute of Japan, Vol. 282, pp. 71-81 (1979)

[2] Architectural Institute of Japan: Generation guide for seismic input motions based on the recent advancement of ground motion studies (2009)

[3] Tokyo Fire Department: The 2011 Tohoku Earthquake Survey (2012)

[4] T. Nakamura, H. Takenaka, T. Okamoto and Y. Kaneda: FDM simulation of seismic wave propagation for an aftershock of the 2009 Suruga Bay earthquake: Effects of oceanbottom topography and sewater layer, Bull. Seism. Soc. Am., Vol. 102, No. 6, pp.2420-2435, (2012)

[5] Central Disaster Prevention Council: "special investigation council concerning Tounankai and Nankai earthquakes, etc." (No. 10), (2003).

[6] Y. Yamamoto and C. Yoshimura: Long-period ground motion simulation of Tokai-Tonankai-Nankai coupled earthquake based on large-scale 3D FEM, Journal of structural and construction engineering. Transactions of AIJ, Vol. 7, No. 677, p.1055-1064, (2012)

[7] D. Baraff: Analytical Methods for Dynamic Simulation of Non-Penetrating Rigid Bodies, Computer Graphics Proceedings(SIGGRAPH 89) Vol. 23, pp. 223-232, 1989.

[8] Kenny Erleben: Multibody Dynamics Animation Lecture 12, http://www.diku.dk/OLD/undervisning/2005f/101/lecture12.pdf .

[9] S. Hasegawa, Y. Tazaki, H. Mitake et al.: "Springhead2", http://springhead.info/wiki/index.php .

TSUBAME

International Research Collaboration

The high performance of supercomputer TSUBAME has been extended to the international arena. We promote international research collaborations using TSUBAME between researchers of Tokyo Institute of Technology and overseas research institutions as well as research groups worldwide.

Recent research collaborations using TSUBAME

1. Simulation of Tsunamis Generated by Earthquakes using Parallel Computing Technique
2. Numerical Simulation of Energy Conversion with MHD Plasma-fluid Flow
3. GPU computing for Computational Fluid Dynamics

Application Guidance

Candidates to initiate research collaborations are expected to conclude MOU (Memorandum of Understanding) with the partner organizations/departments. Committee reviews the "Agreement for Collaboration" for joint research to ensure that the proposed research meet academic qualifications and contributions to international society. Overseas users must observe rules and regulations on using TSUBAME. User fees are paid by Tokyo Tech's researcher as part of research collaboration. The results of joint research are expected to be released for academic publication.

Inquiry

Please see the following website for more details.
http://www.gsic.titech.ac.jp/en/InternationalCollaboration

GSIC
Global Scientific Information
and Computing Center